

A ferromagnetically coupled diphenoxo-bridged $\text{Gd}^{3+}\text{--Mn}^{2+}$ dinuclear complex with a large magneto-caloric effect†‡§

Cite this: *Chem. Commun.*, 2013, **49**, 3845

Received 26th February 2013,
Accepted 22nd March 2013

DOI: 10.1039/c3cc41483c

www.rsc.org/chemcomm

Enrique Colacio,^{*a} José Ruiz,^a Giulia Lorusso,^b Euan K. Brechin^{*c} and Marco Evangelisti^{*b}

A novel diphenoxo-bridged $\text{Gd}^{3+}\text{--Mn}^{2+}$ dimer is proposed as a good candidate for cryogenic magnetic refrigeration. The large MCE is enhanced by the ferromagnetic interaction between the two metal ions.

Heteropolynuclear $3d\text{--Gd}^{3+}$ complexes are attracting much attention because, amongst other things, they have potential application as low-temperature magnetic coolers.¹ These systems show an enhanced magneto-caloric effect (MCE), which is based on the change of magnetic entropy upon application of a magnetic field, that can be exploited for cooling applications *via* adiabatic demagnetisation.¹ The MCE is greatly enhanced in molecules containing isotropic magnetic ions with large total spin S .¹ Taking this into account, $3d/\text{Gd}^{3+}$ complexes are very good candidates for molecular refrigerants as the Gd^{3+} ion has an isotropic f^7 configuration and the $3d\text{--Gd}^{3+}$ magnetic interactions are generally ferromagnetic in nature, leading to ground states with increased and large spin multiplicity.² Moreover, the $3d\text{--Gd}^{3+}$ magnetic exchange interactions are very weak, due to the very efficient shielding of the $4f$ orbitals of the Gd^{3+} by the fully occupied $5s$ and $5p$ orbitals,² and this generates multiple low-lying excited and field-accessible states, each of which can contribute to the magnetic entropy of the system. Another factor favouring a large MCE is the presence of a large metal/ligand mass ratio, in order to limit the amount of passive, non-magnetic elements and in small cluster molecules this is more easily accomplished than in larger ones. Therefore, small, lightweight $3d\text{--Gd}^{3+}$ complexes containing isotropic

transition metal ions such as Mn^{2+} , Fe^{3+} , Cr^{3+} , Cu^{2+} , that exhibit weak ferromagnetic interactions between the metal ions, are appropriate candidates for constructing magnetic coolers.

Although a number of molecular $3d\text{--Gd}^{3+}$ complexes have been reported so far, those containing Mn^{2+} are limited to phosphonate-bridged Mn_4Gd_6 and Mn_9Gd_9 cages,³ one diphenoxo-bridged Mn_2Gd_2 tetranuclear complex,⁴ three triphenoxo-bridged Mn_2Gd trinuclear complexes,⁵ and one alkoxo-bridged MnGd dinuclear complex.⁶ We note that the two former compounds exhibit significant MCE and most exhibit ferromagnetic interactions.

In this communication we report the first example of a diphenoxo-bridged $\text{Gd}^{3+}\text{--Mn}^{2+}$ complex from the compartmental H_2L ligand shown in the inset of Fig. 1, which has an inner pentadentate N_3O_2 coordination pocket and an external O_2O_2 site that favours the formation of $\text{Mn}^{2+}\text{--Ln}^{3+}$. The new compound was predicted to exhibit a ferromagnetic interaction between the metal ions, leading to an enhanced MCE.

The molecular structure of $[\text{Mn}(\text{CH}_3\text{OH})(\mu\text{-L})\text{Gd}(\text{NO}_3)_3]$ (1, Fig. 1) consists of a dinuclear molecule in which the Gd^{3+} and Mn^{2+} ions are bridged by two phenoxo groups of the L^{2-} ligand. Within the dinuclear unit, the Mn^{2+} ion exhibits a [slightly] trigonally distorted MnN_3O_3 coordination polyhedron, where the three N-atoms

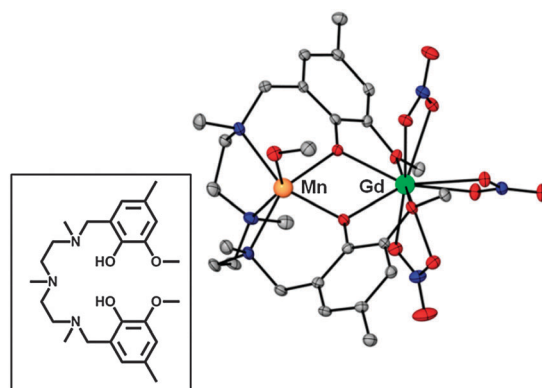


Fig. 1 Perspective view of the molecular structure of **1**. H-atoms are omitted for clarity. Colour code: N = blue, O = red, Mn = orange, Gd = green, C = grey. The inset shows the H_2L pro-ligand.

^a Departamento de Química Inorgánica, Facultad de Ciencias, Universidad de Granada, Av. Fuentenueva S/N, 18071 Granada, Spain. E-mail: ecolacio@ugr.es

^b Instituto de Ciencia de Materiales de Aragón, CSIC-Universidad de Zaragoza, Departamento de Física de la Materia Condensada, 50009 Zaragoza, Spain. E-mail: evange@unizar.es; Web: <http://molchip.unizar.es/>

^c EaStCHEM School of Chemistry, The University of Edinburgh, West Mains Road, Edinburgh, EH93JJ, UK. E-mail: ebrechin@staffmail.ed.ac.uk

† Celebrating 300 years of Chemistry at The University of Edinburgh and 100 years at the University of Granada.

‡ This paper is dedicated to Dr. Jean Pierre Costes on the occasion of his retirement.

§ Electronic supplementary information (ESI) available: Experimental details, crystallographic data in CIF format for **1**, selected bond distance and angles for **1**, energy levels patterns. CCDC 926238. For ESI and crystallographic data in CIF or other electronic format see DOI: 10.1039/c3cc41483c

from the amine groups, and consequently the three O-atoms belonging to the methanol molecule and phenoxo bridging groups, occupy *fac* positions. The Mn–O and Mn–N distances are found in the ranges 2.148(2) Å to 2.158(2) Å and 2.298(3) Å to 2.376(3) Å, respectively. The Gd³⁺ ion exhibits a GdO₁₀ coordination sphere, consisting of the two phenoxo bridging oxygen atoms, the two methoxy oxygen atoms and six oxygen atoms belonging to three bidentate nitrate anions. The GdO₁₀ coordination sphere is rather asymmetric, exhibiting short Gd–O_{phenoxo} bond distances of 2.342(2) Å and 2.322(2) Å, longer Gd–O_{nitrate} bond lengths in the range 2.492(2)–2.522(2) Å and weakly coordinated methoxy groups with Gd–O_{methoxy} distances of 2.608(2) Å and 2.564(2) Å. The Mn(μ-O₂)Gd bridging fragment is almost planar with a hinge angle of 4.1° and rather symmetric with similar pairs of Mn–O bond distances (2.148 Å and 2.158 Å), Gd–O bond distances and Mn–O–Gd bridging angles (110.27° and 110.68°). The Mn···Gd separation is 3.686 Å. In the crystal, molecules are held in pairs by a couple of symmetrically related hydrogen bonds involving the non-coordinated O-atom of one of the bidentate nitrate anions and the methanol molecule, with O···O distances of 2.831 Å (Fig. S1, ESI†). The shortest intermolecular M···M distance is 7.707(1) Å (Mn···Gdⁱ *i* = 2 – *x*, 1 – *y*, 2 – *z*).

The room temperature χ_{MT} value for **1** (12.90 cm³ K mol^{–1}) is slightly higher than the expected value for a pair of non-interacting Mn²⁺ (*S* = 5/2) and Gd³⁺ (*S* = 7/2) ions (12.25 cm³ K mol^{–1}) with *g* = 2. On lowering the temperature χ_{MT} slowly increases from room temperature to 50 K (13.70 cm³ K mol^{–1}) before rising more sharply to reach a quasi-plateau of 19.90 cm³ K mol^{–1} below 3.5 K (see Fig. S2, ESI†). This behaviour is due to a ferromagnetic interaction between the Mn²⁺ and Gd³⁺ ions leading to a *S_T* = 6 spin ground state. The fact that χ_{MT} does not reach the expected value for a *S* = 6 ground state (21.0 cm³ K mol^{–1} for *g* = 2) at 2 K is probably due to the combined result of intermolecular antiferromagnetic interactions, mediated by the hydrogen bonding interactions, and weak zero-field splitting effects from both metal ions. The magnetic properties have been modelled by using the following spin-Hamiltonian:

$$H = -J S_{\text{Gd}} S_{\text{Mn}} - zJ' \langle S_z \rangle S_z + g\mu_{\text{B}} S_{\text{Gd}} B + g\mu_{\text{B}} S_{\text{Mn}} B \quad (1)$$

The first term accounts for the isotropic magnetic exchange coupling between the Mn²⁺ and Gd³⁺ ions, the second accounts for the intermolecular interactions by means of the molecular field approximation, and the last two are the Zeeman terms. The fit of the experimental susceptibility data to the theoretical equation derived from the above Hamiltonian by using the van Vleck equation afforded the following set of parameters: *J* = +0.99(2) cm^{–1}, *g_{Gd}* = 2.02(4), *g_{Mn}* = 2.01(7) and *zJ'* = –0.008(1) cm^{–1}. The *zJ'* parameter also includes the effects of the very weak local anisotropy of Gd³⁺ and Mn²⁺ ions.

Previous DFT calculations^{7,8} and experimental^{2,8} results have clearly shown that the *J_{MnGd}* coupling in diphenoxo-bridged Gd³⁺–M²⁺ complexes (M²⁺ = Mn, Ni, Cu) increases when the planarity of the M–O₂–Gd bridging fragment and the M–O–Gd bridging angle increase. Both structural factors are correlated, so that the latter increases as the bridging fragment becomes more planar. In line with this, compound **1**, with an almost planar Mn–(O)₂–Gd bridging fragment, presents the second largest *J_{MnGd}* value found for ferromagnetically coupled diphenoxo- and triphenoxo-bridged

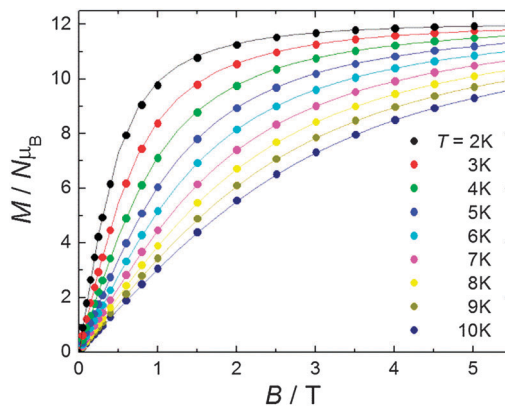


Fig. 2 (Circles) Experimental isothermal magnetization curves for fields up to *B* = 5 T and taken at several *T*, as labelled. The solid lines are the calculated magnetization curves, see the main text for details.

Gd³⁺–Mn²⁺ complexes. Fig. 2 shows the magnetic field dependence of the isothermal magnetization (*M*) for *T* ranging from 2 K to 10 K. The experimental data can be modelled using eqn (1) by neglecting in first instance anisotropies and intermolecular interactions. By using the same values obtained from fitting the susceptibility data, we calculate the magnetization curves (depicted as solid lines in Fig. 2) which nicely account for the experimental data.

The molar heat capacity, *C/R*, measured in the presence of several magnetic fields *B* is plotted in Fig. 3 against temperature. A non-magnetic heat capacity, which we associate to vibrational phonon modes of the lattice, is seen to develop at

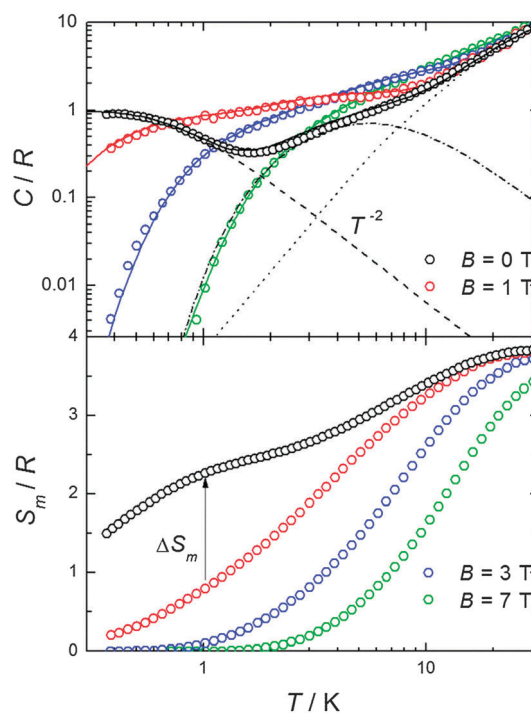


Fig. 3 Top: temperature dependence of the heat capacity *C* normalized to the gas constant *R* and measured in the presence of several magnetic fields, as labelled. Fit of heat capacity (solid lines) is calculated as explained in the text. Lattice (dotted line) and magnetic (dot-dashed lines, dashed lines) contributions are shown. Bottom: experimental magnetic entropies as obtained from the corresponding *C* data.

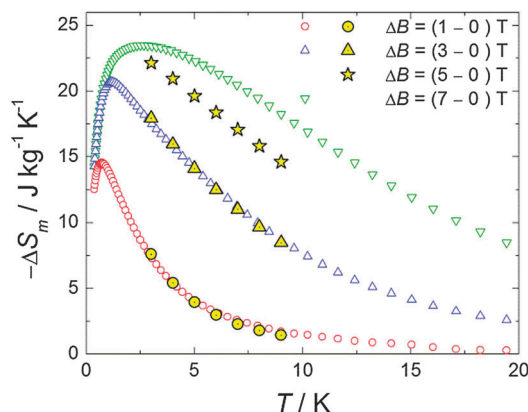


Fig. 4 Temperature-dependencies of the magnetic entropy change ΔS_m , for the indicated applied-field changes ΔB , as obtained from heat capacity (empty markers) and magnetization (full markers) measurements.

high temperatures. The fit to the Debye function (dotted line) gives a Debye temperature $\theta_D = 50.6$ K, in agreement with values reported for this class of material.⁹ At low temperatures, the experimental magnetic heat capacity for $B \geq 1$ T is well described by the calculated Schottky curves as obtained from eqn (1) using the set of eigenvalues found from the fitting of the magnetic data. Intriguingly, the zero-field experimental curve shows two broad Schottky-like features which are well-separated in temperature – being centred at $T \approx 0.3$ K and 5.5 K, respectively. We tentatively explain the anomaly at higher temperatures as the result of the zero-field splitting between the $S_T = 6$ ground state and the first excited level $S = 5$ (dashed-dotted line; see Fig. S3, ESI† for the energy-level diagram). For temperatures lower than ≈ 1 K, only the $S_T = 6$ ground state is populated. In the mean-field approach, the onset of intermolecular magnetic correlations can be interpreted in terms of an interaction field B_{int} , producing a Zeeman splitting of the (otherwise degenerate) $S_T = 6$ ground state leading to an anomaly, as indeed reported in Fig. 4 for such low temperatures. An excellent description of the experimental data is obtained for the interaction field $B_{\text{int}} = 0.16$ T (dashed line in Fig. 3). The solid lines in Fig. 3 are the sum of calculated magnetic and lattice contributions.

An estimate of the magnetic exchange acting between the $S_T = 6$ molecular units can be obtained by comparing the experimental T^{-2} term, $CT^2/R = 0.6$ K² to the theoretical expression for the high-temperature tail of the magnetic heat capacity, *i.e.*, $CT^2/R = 2nz[S(S+1)J'/3k_B]^2$, where z is the number of nearest magnetic neighbours between different $S_T = 6$ molecular units and $n = 1, 2$, and 3 for Ising, XY, and Heisenberg models, respectively.¹⁰ This comparison provides $z^{1/2}|J'|/k_B = 1.5 \times 10^{-2}$ cm⁻¹, in satisfactory agreement with the previous estimate from magnetic data. We note that this value should be considered as an upper estimate for the magnetic exchange since our simple model does not take into account the magnetic dipolar interactions or the magnetic anisotropies. From the heat capacity data we derive the magnetic entropy by making use of the equation:

$$S_m(T, B) = \int_0^T \frac{C_m(T, B)}{T} dT,$$

where C_m is the experimental magnetic heat capacity which we obtain after subtracting the lattice contribution from the total C . This integral is limited by the lowest experimental temperature $T_0 \sim 0.3$ K. For $B = 0$ and 1 T, the lack of experimental data for $T < T_0$ has been accounted for by matching the limiting S_m/R at high T to the full entropy content $\ln(2s_{\text{Gd}} + 1) + \ln(2s_{\text{Mn}} + 1) = 3.87$. From the results depicted in the bottom panel of Fig. 3, it is straightforward to derive the change of magnetic entropy, $\Delta S_m(T, \Delta B = B_f - B_i)$, which characterizes a material in terms of the MCE. Independently, ΔS_m is also obtained from the magnetization data by using the Maxwell relation, *i.e.*,

$$\Delta S_m(T, \Delta B) = \int_{B_i}^{B_f} \left[\frac{\partial M(T, B)}{\partial T} \right]_B dB$$

The results, reported in Fig. 4, show a perfect agreement between the two independent derivations. The MCE for $\Delta B = 7$ T is maximum at $T = 2.7$ K reaching a value of 23.5 J kg⁻¹ K⁻¹.

To summarize, by diagonalizing spin Hamiltonian (1) we have fitted the susceptibility and magnetization data for complex **1** obtaining an intramolecular ferromagnetic exchange coupling between the metal centres. The value so-obtained for the exchange is amongst the largest so far reported for similar dinuclear and trinuclear Mn²⁺–Gd³⁺ compounds. This is attributed to the near planar Mn–(O)₂–Gd bridging fragment.^{7,8} From heat capacity measurements, we found that the magnetic entropy change reaches significant values for 1–3 K, namely $\Delta S_m = 23.5$ J kg⁻¹ K⁻¹ for $\Delta B = 7$ T. Our results therefore suggest that the Gd³⁺–Mn²⁺ molecular dimer **1** is a very good candidate for a magnetic coolant for liquid-helium temperatures.

We are grateful to MINECO (contracts MAT2012-38318-C03 and CTQ2011-24478), EC for a Marie Curie-IEF (PIEF-GA-2011-299356 to GL). EKB thanks the EPSRC and Leverhulme Trust.

Notes and references

- 1 M. Evangelisti and E. K. Brechin, *Dalton Trans.*, 2010, **39**, 4672.
- 2 M. Andruh, J. P. Costes, C. Diaz and S. Gao, *Inorg. Chem.*, 2009, **48**, 3342.
- 3 Y.-Z. Zheng, E. M. Pineda, M. Helliwell and R. E. P. Winpenny, *Chem.-Eur. J.*, 2012, **18**, 4161.
- 4 Y. Bi, Y. Li, W. Liao, H. Zhang and D. Li, *Inorg. Chem.*, 2008, **47**, 9733.
- 5 (a) T. Yamaguchi, J. P. Costes, Y. Kishima, M. Kojima, Y. Sunatsuki, N. Brefuel, J. P. Tuchagues, L. Vendier and W. Wernsdorfer, *Inorg. Chem.*, 2010, **49**, 9125; (b) V. Chandrasekhar, B. M. Pandian, R. Boomishankar, A. Steiner and R. Clérac, *Dalton Trans.*, 2008, 5143; (c) J. P. Costes, J. García-Tojal, J. P. Tuchagues and L. Vendier, *Eur. J. Inorg. Chem.*, 2009, 3801.
- 6 A. N. Georgopoulou, R. Adam, C. P. Raptopoulou, V. Psycharis, R. Ballesteros, B. Abarca and A. K. Boudalis, *Dalton Trans.*, 2010, **39**, 5020.
- 7 E. Cremades, S. Gomez-Coca, D. Aravena, S. Alvarez and E. Ruiz, *J. Am. Chem. Soc.*, 2012, **134**, 10532.
- 8 E. Colacio, J. Ruiz, A. J. Mota, M. A. Palacios, E. Cremades, E. Ruiz, F. J. White and E. K. Brechin, *Inorg. Chem.*, 2012, **51**, 857.
- 9 See for example M. Evangelisti, F. Luis, L. J. de Jongh and M. Affronte, *J. Mater. Chem.*, 2006, **16**, 2534 and references therein.
- 10 A. Abragam and B. Bleaney, *Electron Paramagnetic Resonance of Transition Ions*, Oxford University Press, Oxford, England, 1970.